Magnetic phase diagram and Mott transition of the half-filled $\frac{1}{5}$-depleted Hubbard model with frustration

Atsushi Yamada
Department of Physics, Chiba University, Chiba 263-8522, Japan
(Received 21 August 2014; published 22 December 2014)

The magnetic properties and Mott transition of the half-filled Hubbard model on the $\frac{1}{5}$-depleted square lattice with frustration are studied at zero temperature by the variational cluster approximation. The (π,π) Néel ordering is stable in a wide region of the phase diagram and almost completely veils the nonmagnetic Mott transition for the nonfrustrated case. However, (π,π) Néel ordering is severely suppressed by the frustration, and even with moderate frustrations the nonmagnetic Mott transition takes place in the range where the intradimer hoppings are larger than the intraplaquette hoppings.

DOI: 10.1103/PhysRevB.90.245139 PACS number(s): 71.30.+h, 71.10.Fd, 71.27.+a

I. INTRODUCTION

When the kinetic and Coulomb repulsion energies are competing, low-dimensional materials exhibit a variety of phenomena. Spin liquid is a well-known example, which is discovered in fact in the triangular-lattice organic materials κ-(BEDT-TTF)$_2$X [1–3] and Herbert-smithite ZnCu3(OH)$_6$Cl$_2$ with kagome lattice structure [4,5]. In addition to the phenomena which are directly related to the nonmagnetic Mott transition, strongly correlated systems sometimes take unusual states like the superconductivity near the Mott insulator or the magnetic states which veil the Mott physics. The high-T_c superconductivity [6] is a spectacular example and the superconductivity is also observed in the charge-transfer salts [7–9]. These interesting phenomena are highly dependent on the lattice structure and degree of the geometric frustrations of the systems, and as a theoretical model incorporating the Mott physics the half-filled Hubbard model is actively studied using nonperturbative methods, e.g., on the square [10–18], triangular [20–31], and kagome lattices [32–37], aiming to reveal the phase structure of the system and inspire further material designs. For example, d-wave superconductivity is obtained on the square lattice [10–13], and the nonmagnetic insulator, which is a candidate of the spin liquid, is realized on the triangular [28–31] and kagome lattices [32–37].

One of the interesting lattice structures, not mentioned above, is the $\frac{1}{5}$-depleted square lattice depicted in Fig. 1(a). This lattice structure is realized by CaV_4O_9 [38] and iron selenide families [39], and a similar lattice structure is discussed relating to the iron-chalcogenide family [40]. The $\frac{1}{5}$-depleted square lattice is a non-Brave lattice and its multiband structure will provide greater flexibility in controlling the electronic properties of materials of this lattice structure. In the limit of the infinite Coulomb repulsion, the (π,π) Néel ordering, illustrated in Figs. 1(b) and 1(c), separates two spin gapped states, one adiabatically connected to decoupled dimers, the other connected to decoupled plaquettes, by the second-order quantum transition [41–47]. As for the effect of the electron correlations, the Mott transition was recently studied using the Hubbard model by cluster dynamical mean-field theory (CDMF) [48], but this analysis assumed the nonmagnetic ground state, and if the Mott transition is veiled or not by the (π,π) Néel ordering is not clear. The magnetic properties are investigated by the determinant quantum Monte Carlo [49], which reports that the dominant magnetism is the (π,π) Néel ordering, but the Mott transition was not analyzed. Moreover, the effect of the next-nearest hoppings, which is in general not negligible [45,46] and expected to largely affect the magnetic properties, was not considered in these analyses [48,49]. In this paper we investigate the magnetic phase diagram and Mott transition in the half-filled Hubbard model on the $\frac{1}{5}$-depleted square lattice taking into account the effect of the frustration at zero temperature by the variational cluster approximation (VCA).

We found that the (π,π) Néel ordering (AF) is stable for a wide region of the phase diagram and almost completely veils the nonmagnetic Mott transition for the nonfrustrated case. However, AF is severely suppressed by the frustration, and the nonmagnetic Mott transition is realized for the dimer side $t_1 \lesssim t_2$ even when the frustration is moderate, $0.3 \lesssim t_{3,4}/t_{1,2} \lesssim 0.5$. In the plaquette side $t_2 \lesssim t_1$, AF still veils the nonmagnetic Mott transition for moderate frustrations.

II. $\frac{1}{5}$-DEPLETED SQUARE LATTICE HUBBARD MODEL AND VARIATIONAL CLUSTER APPROXIMATION

The Hamiltonian of the Hubbard model on the $\frac{1}{5}$-depleted square lattice is given by

$$H = -\sum_{i,j,\sigma} t_{ij} c^\dagger_{i\sigma} c_{j\sigma} + U \sum_i n_{i\uparrow} n_{i\downarrow} - \mu \sum_{i,\sigma} n_{i\sigma},$$

where $c_{i\sigma}$ ($c^\dagger_{i\sigma}$) annihilates (creates) an electron with spin σ on the site i, $n_{i\sigma} = c^\dagger_{i\sigma} c_{i\sigma}$ is the electron density, U is the on-site Coulomb repulsion, and μ is the chemical potential. The hopping integrals $t_{i,j} = t_1$ on plaquette bonds, $t_{i,j} = t_2$ on dimer bonds, $t_{i,j} = t_3$ for the next-nearest-neighbor sites within the plaquettes, and $t_{i,j} = t_4$ for the next-nearest-neighbor sites between the plaquettes, as are depicted in Fig. 1(a). We set the energy unit as $t_2 = 1$ for the dimer side $t_1 \leqslant t_2$, and as $t_1 = 1$ for the plaquette side $t_2 \leqslant t_1$. As for the effect of the frustration $t_{3,4}$, we introduce the frustration parameter $f = t_3/t_1 = t_4/t_2$ and consider the three cases $f = 0, 0.3$, and 0.5. When nonfrustrated $f = 0$, the system has a particle-hole symmetry at half filling. For unfrustrated and noninteracting case $f = 0$ and $U = 0$, the ground state is a band insulator for $t_1/t_2 < 0.5$, and it is a metal for $0.5 < t_1/t_2$ [48,50].

We use VCA [51] in our analysis. In this approach, we write the thermodynamic potential of the system $\Omega_{\mathbf{t}}[\Sigma]$ in the

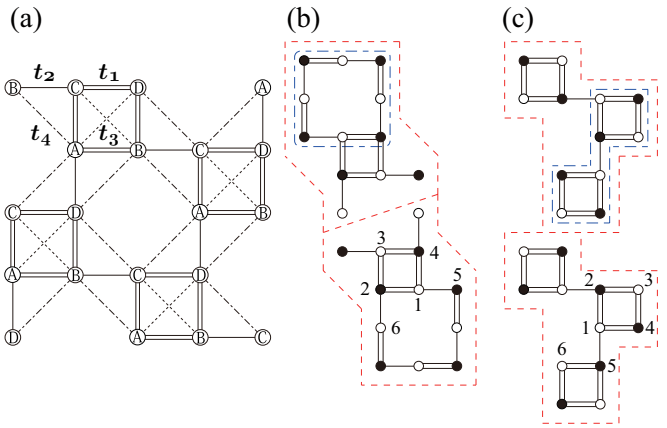

FIG. 1. (Color online) (a) Schematic view of the hopping terms $t_1 \sim t_4$ in the $\frac{1}{5}$-depleted square lattice. (b),(c) The 12-site clusters (the dashed red lines) and 8-site clusters (dash-dotted blue lines) used in VCA. The filled and unfilled circles correspond to up and down spins in the (π,π) Néel ordering, respectively. The 12-site clusters are mirrored to recover the lattice geometry in the analysis of the (π,π) Néel ordering in VCA.

form of a functional of the self-energy Σ, where $\mathbf{t}$ stands for the explicit dependence of $\Omega_{\mathbf{t}}$ on all the one-body operators in the Hamiltonian. This functional $\Omega_{\mathbf{t}}[\Sigma]$ is stationary $\delta\Omega_{\mathbf{t}}[\Sigma]/\delta\Sigma = 0$ at the physical self-energy, and this condition is equivalent to the Dyson's equation for the Green's function. We can evaluate $\Omega_{\mathbf{t}}[\Sigma]$ for the exact self-energy of a simpler Hamiltonian H' which shares the same interaction part with H. As for H', which is referred to as the reference system hereafter, we use the same model defined on the disconnected identical clusters which tile the original infinite clusters. The effect of the symmetry breaking is studied by including various Weiss fields into H'. When the space of the self-energy Σ is restricted to the exact self-energy of H', the functional $\Omega_{\mathbf{t}}[\Sigma]$ is reduced to the function of the one body operators $\mathbf{t}'$ of H', expressed as

$$\Omega_{\mathbf{t}}(\mathbf{t}') = \Omega' - \int_C \frac{d\omega}{2\pi} e^{\delta\omega} \sum_{\mathbf{K}} \ln\det\left[1 + \left(G_0^{-1} - G_0'^{-1}\right)G'\right], \tag{1}$$

where Ω' and G' are the thermodynamic potential and exact Green's function of H', and G_0 and G_0' are the noninteracting Green's function of H and H', respectively. The frequency integral is carried along the imaginary axis $\delta \to +0$ and the sum is over the superlattice wave vectors. The stationary solution of $\Omega_{\mathbf{t}}(\mathbf{t}')$ and the exact self-energy of H' at the stationary point, denoted as Σ^*, are the approximate grand potential and self-energy of H in VCA. Within this framework, we can compute expectation values of one-body operators using the approximate Green's function $G^{-1} = G_0^{-1} - \Sigma^*$. In VCA, the short-range correlations within the reference cluster are exactly taken into account and the restriction of the space of the self-energies Σ into that of H' is the only approximation.

In our analysis, the 8- and 12-site clusters in Figs. 1(b) and 1(c) are used. We refer to these clusters as 8D and 12D [Fig. 1(b)] and 8P and 12P [Fig. 1(c)] hereafter. To investigate the symmetry breaking, we include the Weiss field

$$H_{\mathrm{AF}} = h_{\mathrm{AF}} \sum_i \mathrm{sign}(i)(n_{i\uparrow} - n_{i\downarrow}) \tag{2}$$

into the cluster Hamiltonian, where $\mathrm{sign}(i) = -1$ for the up-spin sites and $\mathrm{sign}(i) = 1$ for the down-spin site in Figs. 1(b) and 1(c). To study the AF ordering on 12D and 12P, we combined these clusters with their mirror images as depicted in Figs. 1(b) and 1(c) to consistently cover the infinite lattice in the presence of the AF ordering. In this case the cluster Green's function G' which appears, e.g., in Eq. (1) is given by

$$G'^{-1} = \sum_i G'^{-1}_i + \tilde{t},$$

where G'_i is the exact Green's function on 12D or 12P, $\tilde{t}$ is the hopping matrix linking the two 12D or 12P clusters, and the site and spin indices are suppressed. We treat h_{AF} and the cluster chemical potential μ' as variational parameters, where μ' has to be included for the thermodynamic consistency [52]. With this setup the variational principle $\delta\Omega_{\mathbf{t}}[\Sigma]/\delta\Sigma = 0$ is reduced to the stationary point search of the grand potential per site $\Omega(\mu',h_{\mathrm{AF}})$ with respect to μ' and h_{AF}. During the search, the chemical potential of the system μ is also adjusted so that the electron density n is equal to 1 within 0.1%. In general, a stationary solution with $h_{\mathrm{AF}} \neq 0$ corresponding to the AF state and that with $h_{\mathrm{AF}} = 0$ corresponding to the nonmagnetic state are obtained, and the energies per site $E = \Omega + \mu n$ are compared between these states to determine the ground state.

On 8D and 12D every site can form a dimer with other sites in the same reference cluster. Similarly, every site can form a plaquette with other sites in the same reference cluster on 8P and 12P. In VCA, the AF ordering is studied by including the Weiss field Eq. (2) in the reference Hamiltonian, and since the formation of the dimers or plaquettes is one of the leading competitors for the AF ordering, for example, the sites in 8P and 12P which cannot form a dimer within the same reference cluster tend to magnetically order easily in the dimer side $t_1 \lesssim t_2$ due to the AF Weiss field, which does not correspond to physical situations. Similar phenomena take place in the plaquette side $t_2 \lesssim t_1$ on 8D and 12D for the sites which cannot form a plaquette within the same reference cluster. In order to circumvent these unphysical situations, we combine the results of the dimer-type cluster 12D and plaquette-type cluster 12P, and identify the AF phase as the region where AF is stable both on 12D and 12P.

For the AF solutions, we compute the magnetic order parameter per site:

$$M = \frac{1}{n_c} \sum_{a=1}^{n_c} \mathrm{sign}(a)(\langle n_{a\uparrow}\rangle - \langle n_{a\downarrow}\rangle),$$

where $\langle n_{a\sigma}\rangle$ is the expectation values of $n_{a\sigma}$ and n_c is the number of the sites in the unit cell in the sense of the sublattice formalism, which is 8 for the AF ordering on the $\frac{1}{5}$-depleted square lattice. For the nonmagnetic solutions, we compute the density of state per site

$$D(\omega) = \lim_{\eta\to 0} \int \frac{d^2k}{(2\pi)^2} \frac{1}{n_c} \sum_{\sigma,a=1}^{n_c} \left\{ -\frac{1}{\pi} \mathrm{Im} G_{a\sigma}(k,\omega + i\eta) \right\} \tag{3}$$

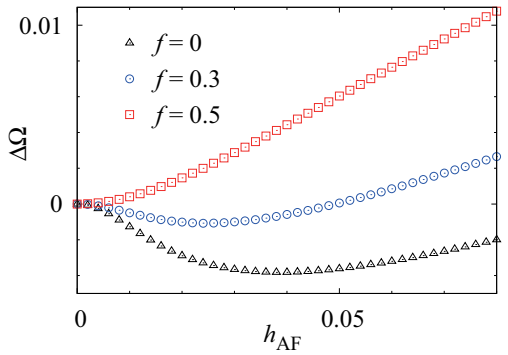

FIG. 2. (Color online) The difference of the grand potentials per site $\Delta\Omega = \Omega(\mu', h_{\rm AF}) - \Omega(\mu', h_{\rm AF} \equiv 0)$ as the function of the Weiss parameter $h_{\rm AF}$ computed on 12D at $t_1/t_2 = 0.85$, $U = 10$, and $\mu = \mu' = 5$. The triangles, circles, and squares correspond to the cases $f = 0$, 0.3, and 0.5, respectively.

to examine the insulating gap, where $G^{-1} = {G_0}^{-1} - \Sigma^*$ is the approximate Green's function in VCA, $n_c = 4$ for the nonmagnetic states, and the k integration is over the corresponding Brillouin zone. In Eq. (3), we evaluate the $\eta \to 0$ limit using the standard extrapolation method by calculating $D(\omega)$ for $\eta = 0.01$, 0.005, and 0.0025. The numerical error after this extrapolation is estimated to be of order 10^{-3}, so the gap is identified as the region of ω around $\omega \simeq 0$ where the extrapolated $D(\omega)$ is less than 10^{-2}. The critical interaction strength $U_{\rm MI}$ of the nonmagnetic Mott transition is determined as the point where the insulating gap closes.

III. MAGNETIC PROPERTIES

Figure 2 shows the difference of the grand potentials per site $\Delta\Omega = \Omega(\mu', h_{\rm AF}) - \Omega(\mu', h_{\rm AF} \equiv 0)$ computed on 12D as the function of the Weiss parameter $h_{\rm AF}$ at $t_1 = 0.85$, $U = 10$, and $\mu = \mu' = 5$. The triangles, circles, and squares correspond to the cases $f = 0$, 0.3, and 0.5, respectively. When $f = 0$ or 0.3 a minimum with $h_{\rm AF} \neq 0$ corresponding to a magnetic solution exists. In fact after the stationary point search with respect to μ' and $h_{\rm AF}$ the magnetic solution gives the energy lower than the nonmagnetic solution with $h_{\rm AF} = 0$, and thus AF is realized at $t_1 = 0.85$ and $U = 10$ for $f = 0$ and 0.3. The potential becomes shallower as the frustration increases and at $f = 0.5$ only the nonmagnetic ground state is obtained. So the nonmagnetic state is realized at $t_1 = 0.85$ and $U = 10$ for $f = 0.5$.

Figure 3 shows the phase diagram with (a) $f = 0$ and (b) $f = 0.5$ computed by VCA. The filled circles correspond to the magnetic transition points U_c computed on 12D and up triangles correspond to the nonmagnetic Mott transition points $U_{\rm MI}$ computed imposing $h_{\rm AF} = 0$ on 12D. The filled squares and down triangles correspond to U_c and $U_{\rm MI}$ on 12P, respectively. The unfilled marks correspond to the results on 8D and 8P. On 12P and 8P the Mott transition points $U_{\rm MI}$ are only slightly larger than the magnetic transition points U_c for $f = 0$, and thus the down triangles overlap with squares or circles in Fig. 3(a). For $t_1/t_2 \leqslant 0.9$, the AF phase on 12P and 8P always extends from rather low U to infinity and is wider than that of 12D and 8D, so the results on 12P and 8P in this

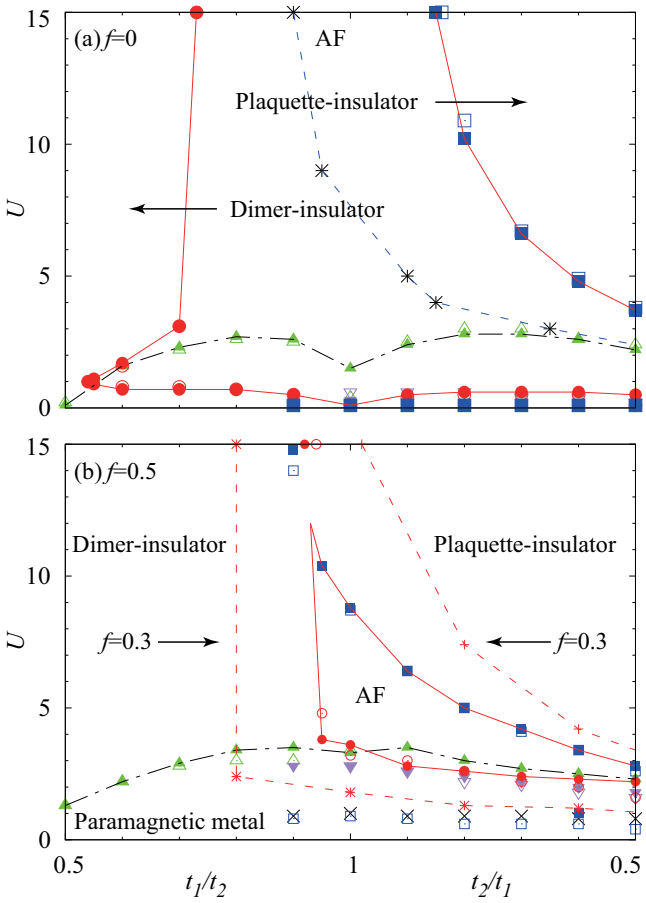

FIG. 3. (Color online) Phase diagram of the Hubbard model on the $\frac{1}{5}$-depleted square lattice with (a) $f = 0$ and (b) $f = 0.5$. The filled circles correspond to the magnetic transition points U_c computed on 12D, and up triangles correspond to the nonmagnetic Mott transition points $U_{\rm MI}$ computed imposing $h_{\rm AF} = 0$ on 12D. The filled squares and down triangles correspond to U_c and $U_{\rm MI}$ on 12P, respectively. The unfilled marks correspond to the results on 8D and 8P. Lines are guides to the eye.

region are not shown in Figs. 3(a) and 3(b) for simplicity. In Fig. 3(a) the asterisks denote the points where the magnetic order parameter M takes its maximum value as the function of t_1/t_2 for fixed U. In Fig. 3(b) the region between the dashed lines corresponds to the AF phase at $f = 0.3$ determined by VCA combining the 12D and 12P results, where the asterisks correspond to U_c computed on 12D and the pluses correspond to U_c computed on 12P. In Fig. 3(b) the crosses denote the points below which the paramagnetic ground state on 12P becomes a spin triplet, and the magnetic properties below these points are not analyzed. On 12P the AF phase persists down to these points for $0.9 \leqslant t_1/t_2$ except at $t_2/t_1 = 0.6$. In Figs. 3(a) and 3(b), there are no energetically disfavored AF, insulator, and metallic solutions around the transition points, which indicates that both the magnetic transition at U_c and nonmagnetic Mott transition at $U_{\rm MI}$ are of the second order.

Comparing Figs. 3(a) and 3(b), AF is stable in a wide region and almost completely veils the nonmagnetic Mott transition for $f = 0$. However, AF is highly suppressed by the frustration, especially in the dimer side, and the nonmagnetic

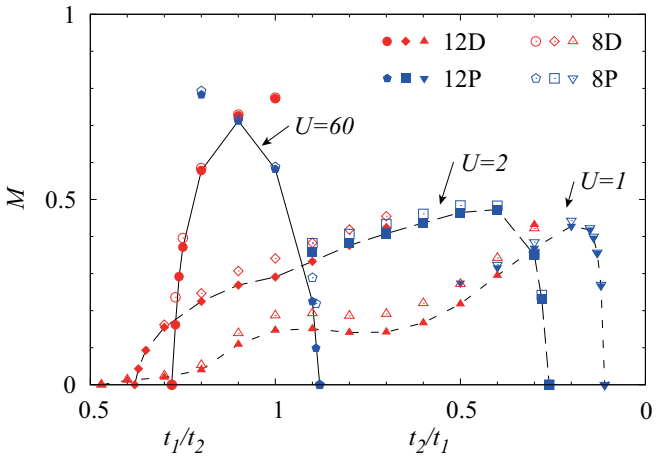

FIG. 4. (Color online) Magnetic order parameter M with $f = 0$ at $U = 60$, 2, and 1 computed by VCA. Lines are guides to the eye, where the lower values of M among 12D and 12P are connected, to circumvent the overestimation.

Mott transition is realized without being veiled by AF in the dimer side. In the plaquette side, the nonmagnetic Mott transition is still veiled by AF even for the frustrated case on all the four clusters. In Fig. 3 we connected the data $U_{\rm MI}$ and U_c of 12D in the region $U \lesssim 3$ even in the plaquette side $1.0 \gtrsim t_2/t_1$. We discuss this point later with the analysis of $\langle S_i \cdot S_j \rangle$ on 12D and 12P; however, our overall conclusions are not affected by this preference since AF veils the Mott transition on all the four clusters in the plaquette side.

The cluster size dependence of the results among the same type of clusters, i.e., between 8D and 12D, or 8P and 12P, is rather small. In general, in VCA, the ordered phase shrinks as the cluster size increases since the spatial fluctuations, which destroy the ordered state, are simulated finer and taken into account more on the larger clusters. As for the nonmagnetic Mott transition points $U_{\rm MI}$, since electrons can move a wider space on larger clusters, average kinetic energy of the electrons becomes lower on the larger clusters, which stabilizes the metallic state and gives rise to the larger $U_{\rm MI}$.

Figure 4 shows the magnetic order parameter M with $f = 0$ at $U = 60$ computed by VCA. Lines are guides to the eye, where the lower values of M among 12D and 12P are connected to circumvent the overestimation due to the unphysical situations discussed previously. After combining the 12D and 12P data, the position of the maximum of M shifts from the dimer side $t_1/t_2 \simeq 0.9$ to the plaquette side $1 > t_2/t_1$ as U decreases.

Here we briefly compare our results for the nonfrustrated case $f = 0$ with other analyses. First we compare our results for large U with the results of the Heisenberg models. In VCA, the critical hopping t_{1c} separating the AF and nonmagnetic phases in the dimer side $t_1/t_2 \leqslant 1.0$ is $t_{1c} = 0.73$ both for $U = 30$ and 60, and the critical hopping t_{2c} separating the AF and nonmagnetic phases in the plaquette side $1.0 \geqslant t_2/t_1$ is $t_{2c} = 0.89$ for $U = 60$ and $t_{2c} = 0.88$ for $U = 30$. The results [43] of the Heisenberg model are $0.74 < t_{1c} < 0.81$ and $0.96 < t_{2c} < 0.98$. The magnetic transition is of the second order and order parameter M takes its maximum at $t_1/t_2 \simeq 0.9$ both in the Heisenberg model [43] and VCA for large U. Therefore the results of the Heisenberg model and VCA with large U agree very well except the value of t_{2c}.

Comparing with the CDMFT [48], our $U_{\rm MI}$ is smaller than that of CDMFT. This tendency is observed also, e.g., on the kagome lattice [36,37], which is another example of the non-Brave lattice. As was stated, in general $U_{\rm MI}$ increases as the cluster size increases in VCA, and since the reference cluster is exactly solved $U_{\rm MI}$ approaches the exact value of the infinite system from below as the cluster size increases in VCA. In this sense $U_{\rm MI}$ in VCA is underestimated compared to the exact result. The Mott transition is of the second order both in VCA and CDMFT for $f = 0$ where the particle-hole symmetry holds at half filling. In general, on other lattices, VCA predicts the second-order Mott transition [19,31,37] while the CDMFT with bath degrees of freedom predicts the first-order phase transition [53]. In the CDMFT, the metallic and insulating states in the coexisting region differ by the value of the hybridization parameter between the cluster and bath degrees of freedom. In VCA, there are no such parameters because there are no bath degrees of freedom.

Comparing with the DQMC [49], our U_c is very similar to that of DQMC, though only the three values of U are analyzed in DQMC. In DQMC the high-symmetry point, defined in [49], shifts from the dimer side to the plaquette side as U decreases.

As for the frustrated case $f \neq 0$, AF is realized with $f = 0.3$ and non-magnetic insulator is realized with $f = 0.5$ at $t_1/t_2 = 1$ for $U = 15$ in Fig. 3(b), and this is quantitatively consistent with the results of the Heisenberg model analysis [47].

To further study the properties of the nonmagnetic state, we analyze, by the exact diagonalization of the reference cluster at the nonmagnetic stationary point of VCA, the correlation $\langle S_i \cdot S_j \rangle$ for different links: along the side of the plaquette P1 $= \langle S_1 \cdot S_2 \rangle$, along the diagonal of the plaquette P3 $= \langle S_1 \cdot S_3 \rangle$, along the dimer D2 $= \langle S_1 \cdot S_5 \rangle$, and along the t_4 direction IP4 $= \langle S_1 \cdot S_6 \rangle$, together with the total spin squared of the dimer SD $= \langle (S_1 + S_5)^2 \rangle$ and that of the plaquette SP $= \langle (\Sigma_{i=1}^4 S_i)^2 \rangle$, where the positions of sites 1–7 on these clusters are depicted in Figs. 1(b) and 1(c). Figures 5(a)–5(b) show the correlation $\langle S_i \cdot S_j \rangle$ computed at $t_1/t_2 = 0.7$ on 12D and at $t_2/t_1 = 0.7$ on 12P. The filled marks correspond to $f = 0.5$ and unfilled marks correspond to $f = 0$. The values of P1, P3, D2, IP4, SD, and SP are zero, zero, -0.75, zero, zero, and 3 in the pure dimer state, and they are -0.5, 0.25, zero, zero, 1.5, and zero in the pure plaquette state.

In Figs. 5(a) and 5(b), the values of $\langle S_i \cdot S_j \rangle$ are close to those of the pure dimer state both for $f = 0$ and 0.5, so the dimer insulator is realized above the magnetic transition or Mott transition points in the dimer side. Similarly, in Figs. 5(b) and 5(c), the values of $\langle S_i \cdot S_j \rangle$ are close to those of the pure plaquette state both for $f = 0$ and 0.5, so the plaquette insulator is realized above the magnetic transition points in the plaquette side. For $U \lesssim 2 \sim 3$, $\langle S_i \cdot S_j \rangle$ rapidly decreases and the frustration enhances this decrease, probably because of the enhancement of the mobility of the electrons due to the frustration, which is observed by the increase of $U_{\rm MI}$ by the frustration in Fig. 3. For $U \lesssim 2 \sim 3$, SP becomes larger than SD even in the plaquette side on 12P and we confirmed that

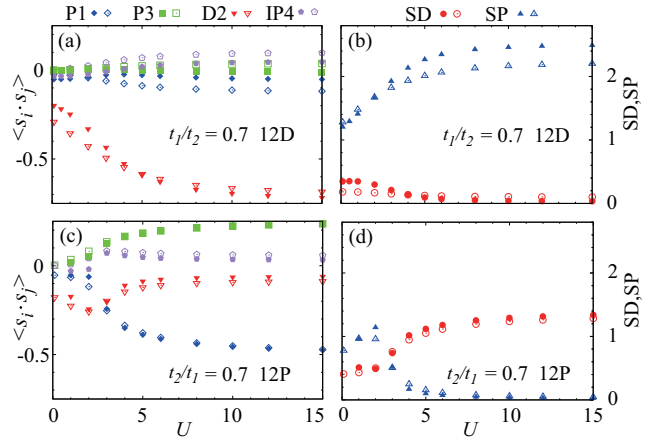

FIG. 5. (Color online) The correlation $\langle S_i \cdot S_j \rangle$ on different links of the reference clusters computed imposing $h_{\mathrm{AF}} = 0$ (a) at $t_1 = 0.7$ on the 12D cluster and (b) at $t_2 = 0.7$ on the 12P cluster. The filled marks correspond to $f = 0.5$ and unfilled marks correspond to $f = 0$.

this behavior is observed also on 12D in the plaquette side. This reverse will be because the maximum value of the total spin squared realized on the four-site plaquette is $2 \times (2 + 1)$ and is larger than that of the two-site dimer $1 \times (1 + 1)$, and SP becomes larger than SD when the spins begin to fluctuate rather freely. This tendency will be too exaggerated on 8P and 12P, which are filled with plaquettes, and this feature leads to the lower U_c and the spin triplet nonmagnetic ground states for small U on 12P. Therefore in the region $U \lesssim U_{\mathrm{MI}}$, the results of 12D will be better approximations of the infinite system even in the plaquette side $1.0 \gtrsim t_2/t_1$ compared to those of 12P.

IV. SUMMARY AND CONCLUSIONS

In summary, we have studied the magnetic phase diagram and Mott transition in the half-filled Hubbard model on the $\frac{1}{5}$-depleted square lattice by VCA, taking into account the effect of the frustrations. We found that the (π,π) Néel ordering is stable in a wide region of the phase diagram and almost completely veils the nonmagnetic Mott transition for the nonfrustrated case. However, the (π,π) Néel ordering is severely suppressed by the frustration and even with moderate frustrations $f \simeq 0.3$–0.5 nonmagnetic Mott transition takes place in the range $t_1/t_2 \lesssim 0.8 \sim 1.0$. The nature of the nonmagnetic insulator phase above the magnetic or Mott transition points is very close to the dimer insulator in the dimer side $t_1/t_2 \lesssim 1.0$, and it is very close to the plaquette insulator in the plaquette side $0.8 \gtrsim t_2/t_1$.

ACKNOWLEDGMENTS

The author would like to thank R. Eder, T. Inakura, H. Kurasawa, H. Nakada, T. Ohama, Y. Ohta, and K. Seki for discussions. Parts of the numerical calculations were performed using the computer facilities of the Institute of Management and Information Technologies at Chiba University, Yukawa Institute at Kyoto University, and the Supercomputer Center at ISSP, University of Tokyo.

[1] S. Lefebvre, P. Wzietek, S. Brown, C. Bourbonnais, D. Jérome, C. Mézière, M. Fourmigué, and P. Batail, Phys. Rev. Lett. **85**, 5420 (2000).
[2] Y. Shimizu, K. Miyagawa, K. Kanoda, M. Maesato, and G. Saito, Phys. Rev. Lett. **91**, 107001 (2003).
[3] F. Kagawa, T. Itou, K. Miyagawa, and K. Kanoda, Phys. Rev. B **69**, 064511 (2004).
[4] J. S. Helton, K. Matan, M. P. Shores, E. A. Nytko, B. M. Bartlett, Y. Yoshida, Y. Takano, A. Suslov, Y. Qiu, J.-H. Chung, D. G. Nocera, and Y. S. Lee, Phys. Rev. Lett. **98**, 107204 (2007).
[5] P. Mendels, F. Bert, M. A. de Vries, A. Olariu, A. Harrison, F. Duc, J. C. Trombe, J. S. Lord, A. Amato, and C. Baines, Phys. Rev. Lett. **98**, 077204 (2007).
[6] J. G. Bednorz and K. A. Muller, Z. Phys. B: Condens. Matter **64**, 189 (1986).
[7] K. Murata, M. Tokumoto, H. Anzai, H. Bando, G. Saito, K. Kajimura, and T. Ishiguro, J. Phys. Soc. Jpn. **54**, 1236 (1985).
[8] N. Tajima, A. Ebina-Tajima, M. Tamura, Y. Nishio, and K. Kajita, J. Phys. Soc. Jpn. **71**, 1832 (2002).
[9] K. Kanoda, J. Phys. Soc. Jpn. **75**, 051007 (2006).
[10] D. Sénéchal, P.-L. Lavertu, M.-A. Marois, and A.-M. S. Tremblay, Phys. Rev. Lett. **94**, 156404 (2005).
[11] M. Aichhorn and E. Arrigoni, Europhys. Lett. **72**, 117 (2005).
[12] H. Yokoyama, M. Ogata, and Y. Tanaka, J. Phys. Soc. Jpn. **75**, 114706 (2006).
[13] M. Aichhorn, E. Arrigoni, M. Potthoff, and W. Hanke, Phys. Rev. B **76**, 224509 (2007).
[14] T. Mizusaki and M. Imada, Phys. Rev. B **74**, 014421 (2006).
[15] A. H. Nevidomskyy, C. Scheiber, D. Sénéchal, and A.-M. S. Tremblay, Phys. Rev. B **77**, 064427 (2008).
[16] T. Yoshikawa and M. Ogata, Phys. Rev. B **79**, 144429 (2009).
[17] S. Yamaki, K. Seki, and Y. Ohta, Phys. Rev. B **87**, 125112 (2013).
[18] L. F. Tocchio, F. Becca, A. Parola, and S. Sorella, Phys. Rev. B **78**, 041101 (2008).
[19] A. Yamada, K. Seki, R. Eder, and Y. Ohta, Phys. Rev. B **88**, 075114 (2013).
[20] P. Sahebsara and D. Sénéchal, Phys. Rev. Lett. **97**, 257004 (2006).
[21] B. Kyung and A. M. S. Tremblay, Phys. Rev. Lett. **97**, 046402 (2006).
[22] T. Ohashi, T. Momoi, H. Tsunetsugu, and N. Kawakami, Phys. Rev. Lett. **100**, 076402 (2008).
[23] A. Liebsch, H. Ishida, and J. Merino, Phys. Rev. B **79**, 195108 (2009).
[24] L. F. Tocchio, A. Parola, C. Gros, and F. Becca, Phys. Rev. B **80**, 064419 (2009).
[25] T. Watanabe, H. Yokoyama, Y. Tanaka, and J. Inoue, Phys. Rev. B **77**, 214505 (2008).
[26] H.-Y. Yang, A. M. Läuchli, F. Mila, and K. P. Schmidt, Phys. Rev. Lett. **105**, 267204 (2010).

[27] A. E. Antipov, A. N. Rubtsov, M. I. Katsnelson, and A. I. Lichtenstein, Phys. Rev. B **83**, 115126 (2011).
[28] T. Yoshioka, A. Koga, and N. Kawakami, Phys. Rev. Lett. **103**, 036401 (2009).
[29] P. Sahebsara and D. Sénéchal, Phys. Rev. Lett. **100**, 136402 (2008).
[30] L. F. Tocchio, H. Feldner, F. Becca, R. Valentí, and C. Gros, Phys. Rev. B **87**, 035143 (2013); L. F. Tocchio, C. Gros, R. Valentí, and F. Becca, *ibid.* **89**, 235107 (2014).
[31] A. Yamada, Phys. Rev. B **89**, 195108 (2014); **90**, 235138 (2014).
[32] Y. Imai, N. Kawakami, and H. Tsunetsugu, Phys. Rev. B **68**, 195103 (2003).
[33] N. Bulut, W. Koshibae, and S. Maekawa, Phys. Rev. Lett. **95**, 037001 (2005).
[34] T. Ohashi, N. Kawakami, and H. Tsunetsugu, Phys. Rev. Lett. **97**, 066401 (2006).
[35] M. Udagawa and Y. Motome, Phys. Rev. Lett. **104**, 106409 (2010); J. Phys.: Conf. Ser. **200**, 012214 (2010).
[36] Y. Furukawa, T. Ohashi, Y. Koyama, and N. Kawakami, Phys. Rev. B **82**, 161101 (2010).
[37] A. Yamada, K. Seki, R. Eder, and Y. Ohta, Phys. Rev. B **83**, 195127 (2011).
[38] S. Taniguchi, T. Nishikawa, Y. Yasui, Y. Kobayashi, M. Sato, T. Nishioka, M. Kontani, and K. Sano, J. Phys. Soc. Jpn. **64**, 2758 (1995).
[39] B. Weil, H. Qing-Zhen, C. Gen-Fu, M. A. Green, W. Du-Ming, H. Jun-Bao, and Q. Ming, Chinese Phys. Lett. **28**, 086104 (2011); F. Ye, S. Chi, Wei Bao, X. F. Wang, J. J. Ying, X. H. Chen, H. D. Wang, C. H. Dong, and M. Fang, Phys. Rev. Lett. **107**, 137003 (2011).
[40] J. K. Glasbrenner, J. P. Velev, and I. I. Mazin, Phys. Rev. B **89**, 064509 (2014).
[41] N. Katoh and M. Imada, J. Phys. Soc. Jpn. **64**, 4105 (1995).
[42] K. Ueda, H. Kontani, M. Sigrist, and P. A. Lee, Phys. Rev. Lett. **76**, 1932 (1996).
[43] M. Troyer, H. Kontani, and K. Ueda, Phys. Rev. Lett. **76**, 3822 (1996).
[44] M. Troyer, M. Imada, and K. Ueda, J. Phys. Soc. Jpn. **66**, 2957 (1997).
[45] O. A. Starykh, M. E. Zhitomirsky, D. I. Khomskii, R. R. P. Singh, and K. Ueda, Phys. Rev. Lett. **77**, 2558 (1996).
[46] M. P. Gelfand, Z.Weihong, R. R. P. Singh, J. Oitmaa, and C. J. Hamer, Phys. Rev. Lett. **77**, 2794 (1996).
[47] M. Albrecht, F. Mila, and D. Poilblanc, Phys. Rev. B **54**, 15856 (1996).
[48] Y. Yanagi and K. Ueda, Phys. Rev. B **90**, 085113 (2014).
[49] E. Khatami, R. R. P. Singh, W. E. Pickett, and R. T. Scalettar, Phys. Rev. Lett. **113**, 106402 (2014).
[50] Y. Yamashita, M. Tomura, Y. Yanagi, and K. Ueda, Phys. Rev. B **88**, 195104 (2013).
[51] D. Sénéchal, D. Perez, and M. Pioro-Ladriére, Phys. Rev. Lett. **84**, 522 (2000); D. Sénéchal, D. Perez, and D. Plouffe, Phys. Rev. B **66**, 075129 (2002); M. Potthoff, M. Aichhorn, and C. Dahnken, Phys. Rev. Lett. **91**, 206402 (2003); C. Dahnken, M. Aichhorn, W. Hanke, E. Arrigoni, and M. Potthoff, Phys. Rev. B **70**, 245110 (2004); M. Potthoff, Eur. Phys. J. B **32**, 429 (2003).
[52] M. Aichhorn, E. Arrigoni, M. Potthoff, and W. Hanke, Phys. Rev. B **74**, 024508 (2006).
[53] M. Potthoff, Eur. Phys. J. B **36**, 335 (2003); M. Balzer, M. Kyung, D. Sénéchal, A. M. Tremblay, and M. Potthoff, Europhys. **85**, 17002 (2009).